Evaluation and Improvement of Generalization Performance of SAR Ship Recognition Algorithms

Chi Zhang, Xi Zhang, Jie Zhang, Gui Gao, *Member, IEEE*, Yongshou Dai, Genwang Liu, Yongjun Jia, Xiaochen Wang, Yi Zhang, and Meng Bao

***Abstract*—As artificial intelligence continues to advance, deep learning has greatly contributed to the advancement of ship recognition using synthetic aperture radar (SAR) images. Deep learning-based SAR ship recognition performance is largely dependent on the sample set used. SAR ship recognition datasets published in recent years, however, are most derived from a single SAR satellite sensor. It needs to be evaluated and analyzed carefully whether the model trained by a single satellite dataset can still achieve the same accuracy with different SAR satellites. This article focuses on the following research to address these issues. First, using multiple SAR satellite sensors, we create a new SAR ship dataset (named generalization performance evaluation dataset, GPED) containing multiresolution and multipolarization data to examine the generalization performance of the deep learning-based SAR ship recognition method. GPED and a marine target detection dataset (MTDD) are then used to evaluate and analyze the generalization performance of current mainstream deep learning methods. According to the the experiment results, the mean average accuracy of the ship recognition model trained on GPED is generally higher than that of MTDD, which proves that the GPED has a better generalization performance. Furthermore, SAR ship detection datasets have more samples than ship recognition datasets, which inspired us to use transfer learning to transfer knowledge from ship detection to ship recognition. In this article, a method for ship recognition based on transfer learning that utilizes the knowledge gained from the ship detection task is proposed. The method includes two modules: 1) pretraining module and 2) fine-tuning module. It can apply samples of unlabeled ship types to ship recognition, thus reducing the number of labeled samples that are required for ship recognition. The experimental results on GPED and MTDD show that our method can achieve good recognition performances.**

***Index Terms*—Deep learning, generalization performance, ship recognition, synthetic aperature radar (SAR), transfer learning.**

I. Introduction

AS THE most important carrier of human maritime activities, ships play an important role in a variety of maritime affairs, such as border control, environmental protection, traffic monitoring, and rescue [1]. Synthetic aperture radar (SAR) is an all-time and all-weather microwave imaging radar that is widely employed for ship detection and recognition. In addition, the rapid development of satellite technology has caused an increase in the number of SAR satellites. With the launches of TerraSAR-X, Sentinel-1, GF-3 (Gaofen-3), and other satellites, SAR has gradually become the primary data source for ship detection and recognition [2].

Recently, many ship detection methods, such as the constant false alarm rate (CFAR) method, have been developed [3]. This algorithm determines the discrimination threshold between the background and the target by setting a constant false alarm rate to achieve fast target detection. Because the detection accuracy of the CFAR method is dependent on the sea clutter model [4], several improved CFAR algorithms, including the smallest of CFAR (SO-CFAR) [5], variability Index CFAR (VI-CFAR) [6], ordered-statistic CFAR (OS-CFAR) [7], and trimmed-mean CFAR (TM-CFAR) [8], have been developed. In addition, ship detection methods based on ship features are widely utilized. Common ship features include geometric features [9], [10], [11], [12], orientation features [13], structural features [14], [15], polarization features [16], [17], [18], [19], [20], and scattering features [21], [22], [23]. Recently, Zhu et al. [24] proposed a projection shape template-based ship recognition method. An efficient feature extraction and classification algorithm based on a visual saliency model is proposed in [25]. Amrani et al. [26] extracted the histogram of oriented gradients (HOG) feature of the target and obtained new discriminant features based on bag of visual words (BOVW) model and discriminant correlation analysis (DCA). The method in [27] employs the BOVW and support vector machine (SVM) for SAR target classification.

With the development of artificial intelligence in recent years, deep learning methods have become prevalent in ship detection,

Manuscript received 15 July 2022; revised 25 September 2022; accepted 17 October 2022. Date of publication 25 October 2022; date of current version 8 November 2022. This work was supported in part by the National Natural Science Foundation of China under Grant 61971455, Grant U2006207, Grant 42106177, and Grant 62131019, in part by the Shandong Provincial Natural Science Foundation of China under Grant ZR2021QF093, and in part by the State Key Laboratory Foundation of CEMEE under Grant CEMEE2022K0303B. *(Corresponding author: Xi Zhang)*.

Chi Zhang and Jie Zhang are with the College of Oceanography and Space Informatics, China University of Petroleum, Qingdao 266580, China, and also with the First Institute of Oceanography, Ministry of Natural Resources, Qingdao 266061, China (e-mail: zc0621@fio.org.cn; zhangjie@fio.org.cn).

Xi Zhang, Genwang Liu, and Meng Bao are with the First Institute of Oceanography, Ministry of Natural Resources, Qingdao 266061, China (e-mail: xi.zhang@fio.org.cn; liugenwang@fio.org.cn; 15092266356@163.com).

Gui Gao is with the Faculty of Geosciences and Environmental Engineering, Southwest Jiaotong University, Chengdu 611756, China (e-mail: dellar@126.com).

Yongshou Dai is with the College of Oceanography and Space Informatics, China University of Petroleum, Qingdao 266580, China (e-mail: daiys@upc.edu.cn).

Yongjun Jia and Yi Zhang are with the National Satellite Ocean Application Service, Ministry of Natural Resources, Beijing 100080, China (e-mail: jiayongjun@mail.nsoas.org.cn; zhangyi@mail.nsoas.gov.cn).

Xiaochen Wang is with the Key Laboratory of Technology in Geo-spatial Information Processing and Application Systems, Aerospace Information Research Institute, Chinese Academy of Science, Beijing 100190, China (e-mail: wangxc@radi.ac.cn).

Digital Object Identifier 10.1109/JSTARS.2022.3216623

TABLE I
DETAILED DESCRIPTIONS OF FIVE OPEN SAR SHIP DETECTION DATASETS

Dataset	Sensor	Polarization	Resolution (m)	Number of ship slices	Reference
SSDD	Sentinel-1, RADARSAT-2	HH, HV, VV, VH	1-15	1160	Li et al. [38]
SAR-Ship-Dataset	GF-3, Sentinel-1	HH, HV, VV, VH	5×5, 8×8, 10×10, etc.	43819	Wang et al. [39]
AIR-SARShip-1.0	GF-3	HH, VV	1, 3	31	Sun et al. [40]
HRSID	Sentinel-1, TerraSAR-X	HH, HV, VV	0.5, 1.3	5604	Wei et al. [41]
LS-SSDD-v1.0	Sentinel-1	VV, VH	5×20	9000	Zhang et al. [42]

which somewhat helps alleviate the shortcomings of traditional methods. In addition, several object detection methods have been developed through convolutional neural networks (CNNs), including the faster region CNN (faster R-CNN) [28], single shot multibox detector (SSD) [29], you only look once (YOLO) [30], and RetinaNet [31]. In addition to the above anchor-based methods, anchor-free methods are also widely used. CornerNet [32] and CenterNet [33] are new methods based on key point detection. The former focuses on the corner points of the bounding box and the latter focuses on the center point of the bounding box. FCOS [34] and Foveabox [35] are also classic anchor-free methods, which predict the position of target bounding box pixel by pixel. Moreover, researchers proposed target detection algorithms based on attention mechanism to improve the detection accuracy of small targets, including DETR [36], ViT [37], etc.

Deep learning-based algorithms rely on a large number of training samples. Therefore, several SAR ship detection datasets (as shown in Table I) have been presented, which further promotes the development of SAR ship detection methods that are based on deep learning. For example, Li et al. [38] produced an SAR ship detection dataset (SSDD) that contains 1160 SAR images. Wang et al. [39] produced the SAR-ship-dataset, which is a larger-scale SAR ship detection dataset for complex scenes that consist of 43 819 ship slices. Sun et al. [40] published an SAR ship detection dataset (AIR-SARShip-1.0) for high resolution, which consists of 31 GF-3 images. Wei et al. [41] constructed a high-resolution SAR ship detection dataset (HRSID) with 5604 images and 16 951 ship slices. Zhang et al. [42] released a large-scale SAR ship detection dataset (LS-SSDD-v1.0) for small ship detection, which contains 15 images from Sentinel-1.

Through the above datasets, researchers have carried out much work on SAR ship detection. For example, Kang et al. [43] used a deep neural network for SAR ship detection and introduced contextual features based on a CNN, which significantly improved the detection performance. Zhang et al. [44] proposed a lightweight feature optimizing network (LFO-Net) that is based on the SSD algorithm and verified the effectiveness of this method by using an SSDD. Lin et al. [45] proposed an improved faster R-CNN algorithm that is based on the channel attention mechanism for ship detection. Chang et al. [46] applied YOLOv2 [47] to SAR ship detection. Wang et al. [48] employed RetinaNet for GF-3 image ship detection. Hou et al. [49] introduced the squeeze and excitation (SE) module into RetinaNet to improve the precision of ship detection. Tang et al. [50] proposed a ship detection method called N-YOLO (Noise-YOLO). Hu et al. [51] presented a dual-polarmetric SAR dataset and a weakly supervised ship detection method based on anomaly detection via advanced memory-augmented autoencoder. Amrani et al. [52] proposed a very deep CNN (VDCNN) method by using small filters to reduce the noise affect and improve the performance.

With advancements in SAR satellite technology progressing, the number of SAR satellites is increasing, and the resolution of SAR images is continuously improving. As a result, finely recognizing different ship types has become an important research topic. Consequently, some scholars have constructed SAR ship recognition datasets (see Table II) and utilized deep learning methods to identify ships. For example, Xing et al. [53] constructed a high-resolution SAR ship dataset (HR-SAR) based on six TerraSAR-X stripmap-mode SAR images and employed a sparse representation method to classify ships. Huang et al. [54] assembled an SAR ship recognition dataset, OpenSARShip, which consists of 41 Sentinel-1 images and 17 types of ships. He et al. [55] deployed dense CNNs to classify ships, presented a multitask learning framework, and carried out an experiment that is based on OpenSARShip, which indicates that the method has excellent performance. Hou et al. [56] published the FUSAR dataset, which contains 126 scenes, 15 major ship classes, and 98 subcategories, and implemented a CNN to classify the ships. Ma et al. [57] constructed a maritime target detection dataset (MTDD) based on GF-3 satellite containing six types and proposed a single shot multibox detector with a multiresolution input (MR-SSD) for ship detection and recognition. Lei et al. [58] released a high-resolution SAR ship recognition dataset SRSDD-v1.0, which consists of GF-3 stripmap-mode SAR images with 1-m resolution and 666 ship slices and utilized eight advanced deep learning detectors to evaluate the dataset. Moreover, Zhang et al. [59] proposed a polarization fusion network with geometric feature embedding for ship classification. Amrani et al. [60] proposed an SAR target recognition method based on YOLO and multicanonical correlation analysis. In [61], the extracted deep features are fused by using DCA algorithm and the K-nearest neighbors algorithm is used for SAR target classification.

However, the above datasets all use a single type of SAR satellite as the data source. The generalization performance of these datasets needs to be evaluated. We obtained a TerraSAR-X image at 22:53:46, 7 January 2012 and a RADARSAT-2 image at 22:51:10, 7 January 2012 of the Straits of Malacca. In this pair of data, the interval between acquisition times of TerraSAR-X and RADARSAT-2 data is about 3 min. Moreover, we matched SAR with automatic identification system (AIS) data and got 62 pairs of ships. Fig. 1 shows the SAR images of two pairs of ships after normalization, where the legend shows the information of

TABLE II
DETAILED DESCRIPTIONS OF FIVE OPEN SAR SHIP RECOGNITION DATASETS

Dataset	Sensor	Polarization	Resolution (m)	Number of ship slices	Reference
HR-SAR	TerraSAR-X	HH, HV, VV	2×1.5	450	Xing et al. [53]
OpenSARShip	Sentinel-1	VH, VV	3×22, 20×22	11346	Huang et al. [54]
FUSAR	GF-3	HH, HV, VH, VV	1.124, 1.7-1.754	5243	Hou et al. [56]
MTDD	GF-3	HH, HV, VH, VV	0.5-5	1727	Ma et al. [57]
SRSDD-v1.0	GF-3	HH, VV	1	666	Lei et al. [58]

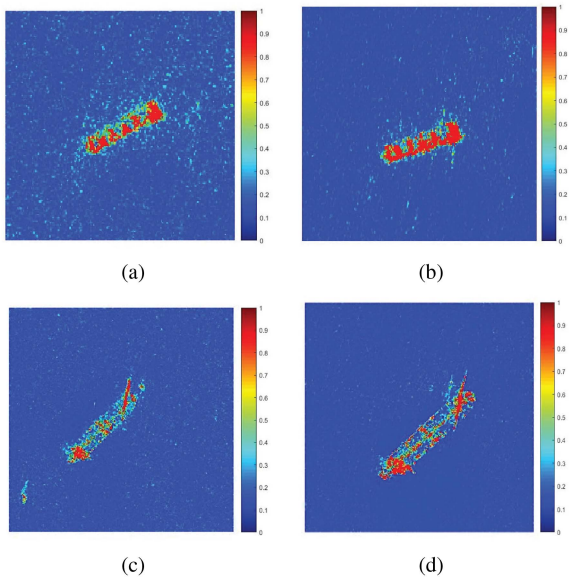

Fig. 1. Differences of the same ship in different satellite images, where (a) and (b) show the same cargo ship, (c) and (d) show the same tanker ship. The legend shows the scattering intensity after normalization. (a) Images of cargo ship in RADARSAT-2. (b) Images of cargo ship in TerraSAR-X. (c) Images of tanker in RADARSAT-2. (d) Images of tanker in TerraSAR-X.

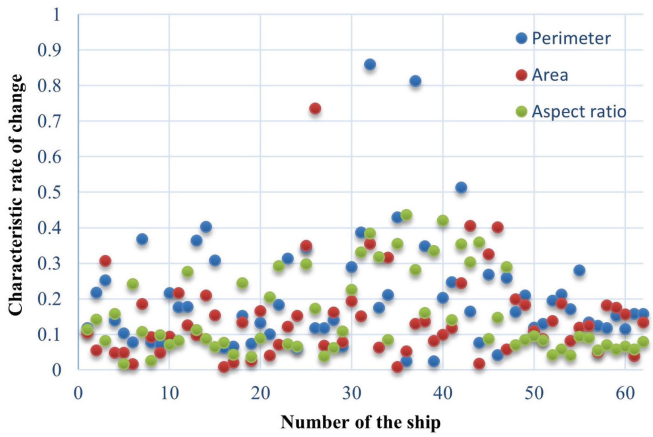

Fig. 2. Difference in the geometric features of same ship targets in TerraSAR-X and RADARSAT-2 images. Characteristic rate of change represents the ratio of the difference between RADARSAT-2 and TerraSAR-X ship characteristics to the ship characteristics of RADARSAT-2.

the intensity change of the scattering point of the ship. It can be seen that the scattering point distribution of the same ship in different SAR images has some differences. Such differences may affect the appearance of the ship features that were extracted from the SAR images [62], [63]. Moreover, we analyzed the difference in the geometric features of the same ship target in the TerraSAR-X image and the RADARSAT-2 image, where the geometric features include the ship's perimeter, area, and aspect ratio. We obtain the length and width of the ship by visual interpretation of the ship in the SAR image, and then calculate the area, perimeter, and aspect ratio of the ship. The ratio of the difference between RADARSAT-2 and TerraSAR-X ship characteristics to the ship characteristics of RADARSAT-2 is used to express the rate of change of characteristics of the same ship. Fig. 2 shows the rate of change of characteristics of 62 pairs of ships. It can be seen from Fig. 2 that there are about 32 ships with a characteristic rate of change greater than 30%. Therefore, the geometric features of same ship targets in different SAR satellite images vary greatly, which may affect the accuracy of ship classification. To further analyze the generalization performance of multidata source datasets, a generalization performance evaluation dataset (GPED) based on SAR images from multiple satellites was constructed in this article. Moreover, to evaluate the generalization performance of datasets constructed from a single satellite image and those constructed from multiple satellite images, we conducted experiments on GPED and MTDD using mainstream deep learning methods. Alternatively, the number of labeled samples also has a great impact on the accuracy of ship recognition. To improve the accuracy of ship recognition without increasing the complexity of the model, ship recognition based on transfer learning is proposed. Transfer learning applies knowledge from source domain to target domain. The source domain generally has sufficient labeled data, while the target domain has scarce labeled data. The natural image domain is usually selected as the source domain because there are a large number of samples in the natural image dataset, such as ImageNet [64]. Natural images refer to the pictures taken by optical cameras commonly used in the field of computer vision. There are more than 14 million natural images in the ImageNet. Several recent works applied transfer learning to SAR ship recognition. For example, Wang et al. [65] utilized the natural image domain as the source domain and achieved cross-domain knowledge migration from the natural image domain to the SAR image domain based on the PASCAL VOC dataset. Rostami et al. [66] selected the optical remote sensing image domain as the source domain and employed the optical ship detection dataset for knowledge migration. Although natural images, optical remote sensing images, and SAR images describe the same physical world,

the imaging mechanisms of natural images and optical remote sensing images are very different from those of SAR images. Thus, natural images, optical remote sensing images, and SAR images significantly vary in data distribution. The difference in data distribution between the source domain and the target domain may lead to a very large domain mismatch problem when knowledge is transferred [67]. In addition, some scholars transferred data from AIS [68] domain to the SAR domain to improve the accuracy of ship detection and recognition [69], [70], [71], [72]. However, such methods require complex data association and matching techniques, which increases the complexity of transfer learning. To solve the problem of domain mismatch, some researchers proposed the domain adaptation method, which entails preprocessing data in the source or target domain to ensure that these data have similar probability distributions. However, the method needs to establish the model of the intermediate embedding space, which increases the complexity of the algorithm [73].

As a result, considering that the number of samples in SAR ship detection datasets is much more than that in ship recognition datasets, an SAR ship recognition method based on transfer learning is proposed in this article. It can be found that all datasets in Table I have a total of 59 614 ship slices, and all datasets in Table II have a total of 19 432 ship slices. In the method, both the source task and the target task belong to the SAR image domain, which effectively avoids the domain mismatch problem caused by the different data distributions. Moreover, the research objects of both the source task and target task are ships, which have common features. The ship features in ship detection task are equally effective in ship recognition task and can be transferred to ship recognition task. Therefore, the proposed method can apply ship samples with unlabeled type to ship recognition, thereby realizing knowledge transfer from ship detection tasks to ship recognition tasks.

In conclusion, the main contributions of this article are shown as follows. First, a generalized performance evaluation dataset is constructed to evaluate the generalization performance of datasets constructed using multiple data sources and datasets constructed using one data source. Second, a task transfer method for SAR ship recognition is proposed, which can apply samples of unlabeled ship types in SAR ship detection dataset to ship recognition and reduce the number of labeled samples that are required for ship recognition. The method can achieve knowledge migration from a ship detection task of a single type to a ship recognition task of multiple types. The previous research is to transfer knowledge in different fields, while we transfer knowledge between different tasks in the same field. The superiority of the proposed method is proved by comparing with other former transfer learning cases through experiment testing on the GPED and MTDD.

The rest of this article is organized as follows. First, we introduce MTDD and the process of constructing the GPED in Section II. Second, we introduce six deep learning algorithms employed in this article and the performance evaluation index in Section III. Third, we evaluate the generalization performance of deep learning algorithms based on MTDD and the GPED and analyze the experimental results in Section IV. We introduce the methods proposed in this article, conduct comparative experiments, and analyze the experimental results in Section V. Finally, Section VI concludes this article.

II. Datasets

A. MTDD

Published by Ma et al. [57] in 2018, MTDD is a marine target detection dataset that includes 1727 ship slices. The size of each slice is 500×500. These samples are obtained from 111 large-scale SAR SLC images of GF-3 satellite, which carries a C-band radar sensor working at 12 imaging modes. These 111 GF-3 SAR images are captured from the offshore areas of Eastern Asia, Western Asia, Western Europe, and Northern Africa. All of them are acquired from December 2016 to May 2018. Samples of MTDD have four types of polarization (HH, HV, VH, and VV), with ground resolution from 0.5 to 5 m. MTDD contains six types of targets, which are mainly cargo, container, tanker, tower, platform, and windmill. There are 913 cargo ships, 147 container ships, and 240 tankers in MTDD.

B. Construction of the GPED

The SAR images used to construct the GPED were obtained from multisource SAR satellites, such as RADARSAT-2, Sentinel-1 A, GF-3 in the C-band, and TerraSAR-X in the X-band. The information of these satellites is shown in Table III. A total of 94 SAR images were acquired, which are mainly distributed in the Bohai Sea, the Yangtze River Delta, the southeast coast of the Jiaodong Peninsula, the Strait of Malacca, and the major ports in Japan. The SAR images were saved in tag image file format (TIFF), and all data were processed by geometric correction and radiometric correction.

The original SAR image covers a wide area, which complicates the sample labeling and increases the computer's memory burden. Therefore, we cropped the original SAR images into ship slices of suitable size. Due to the difference in the resolution of the SAR images from distinct data sources, the size of the ship slices ranged from 50×50 pixels to 200×200 pixels. We saved the ship slices in JPEG format for easy labeling and modified them with linear stretching. Last, 2441 ship slices were obtained.

In this article, sample annotations of the ship slices were performed with the ship type information provided by the AIS. Selecting the imaging time of the SAR image as the center, we obtained AIS data in the same area within 30 min. Considering that the AIS acquisition time and the SAR acquisition time do not exactly coincide and that the position of the ships may deviate, linear interpolation and extrapolation processes were performed to unify the temporal and spatial positions of the AIS with SAR images. For moving ships, due to the influence of the Doppler frequency shift, there is also position variation in the azimuth direction of the image. Thus, compensating for the Doppler frequency shift of moving ships is necessary. The LabelImg [74] tool was used to label the ship target, and the labeling range was the smallest outer rectangle of the ship. All ship slices were manually annotated by SAR interpretation experts. The annotation of ships was stored in extensible markup language

TABLE III
INFORMATION ON SAR DATA OF THE GPED

Satellite	Polarization	Resolution (m)	Incident angle (°)	Number of images
RADARSAT-2	HH, VH, VV	3/5/25	22.1∼43.3	27
Sentinel-1A	VH, VV	10	35.6∼45.8	3
TerraSAR-X	HH, HV, VV	3/8	29.6∼45.5	20
GF-3	HH, HV, VH, VV	3/5/8/10/25	15.2∼50.3	44

TABLE IV
COMPARISON OF MTDD AND GPED

Dataset	Data Source	Polarization	Resolution(m)	Categories	Number of ship slices
MTDD	GF-3	HH, VV, VH, HV	0.5∼5	6	1727
GPED	RADARSAT-2, Sentinel-1A, TerraSAR-X, GF-3	HH, VV, VH, HV	3∼25	16	2441

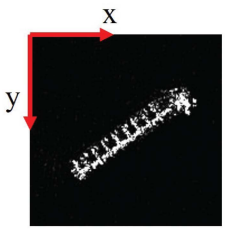


```
<annotation>
        <folder>TSX_HH_8m</folder>
        <filename>IDM_TSX_441381000.jpg</filename>
        <path>F:\IDM_TSX_441381000.jpg</path>
        <source>
                <database>Unknown</database>
        </source>
        <size>
                <width>172</width>
                <height>171</height>
                <depth>1</depth>
        </size>
        <segmented>0</segmented>
        <object>
                <name>cargo</name>
                <pose>Unspecified</pose>
                <truncated>0</truncated>
                <difficult>0</difficult>
                <bndbox>
                        <xmin>32</xmin>
                        <ymin>44</ymin>
                        <xmax>151</xmax>
                        <ymax>131</ymax>
                </bndbox>
        </object>
</annotation>
```

Fig. 3. Example of a ship sample in GPED.

(XML) format, and the specific information is shown in Fig. 3 , which mainly includes the name and size of the ship slice and the type of ship.

After the above steps, there are 2441 ship slices in the GPED. There are 16 types of ships in the GPED, including cargo ships, tankers, passenger ships, rescue ships, etc. The number of samples for cargo ships, container ships, and tankers is high, while the number of samples for other ship types is low.

C. Comparision of MTDD and GPED

The major difference between the GPED and MTDD is that the GPED employs SAR images from multiple data sources, while MTDD only uses SAR images from GF-3. The polarization modes and image resolution of different SAR satellites vary, which causes MTDD and the GPED to differ regarding specific image parameters. Table IV shows the difference between the GPED and MTDD in image parameters. Moreover, both MTDD and the GPED suffer from category imbalance. During the training process, deep learning models typically focus more on the types with a larger number of samples and disregard the types with a smaller number of samples [75]. Thus, the classification accuracy for categories with a smaller number of samples can be very poor, which lowers the average recognition accuracy and affects the stability of the evaluation results. Therefore, we screened the sample types in the original dataset before conducting experiments and selected three types of samples with larger numbers from the original dataset, including cargo ships, container ships, and tankers. The experiments in this article were conducted on the screened dataset. The GPED and MTDD that are subsequently mentioned are the screened GPED and screened MTDD, respectively. The processed MTDD contains 1300 samples that consist of 913 cargo ships, 147 container ships, and 240 tankers. The processed GPED contains 1557 samples, including 810 cargo ships, 505 tankers, and 242 container ships. These three ship categories are also the most common in SAR ship recognition because of their different scattering properties [76]. As shown in Fig. 4, under ideal conditions, cargo ships exhibit black and white stripes and have obvious ship margins. Container ships have stronger black and white stripes than cargo ships and exhibit irregular strong scattering when the containers are loaded. Tankers have obvious symmetry in their scattering characteristics. In addition, Fig. 4 shows some examples from the GPED that are difficult to distinguish and disturbed by backgrounds, such as sea clutter, cross-sidelobe, and defocusing phenomena. These samples increase the difficulty of ship recognition.

III. METHOD OF GENERALIZATION PERFORMANCE EVALUATION

A. Ship Recognition Algorithm Based on Deep Learning

To evaluate the generalization performance of the GPED and MTDD, eight ship recognition algorithms based on deep learning were employed in this article. The model structure and principle of these eight algorithms are introduced as follows.

1) Faster R-CNN: Faster R-CNN [28] is a two-stage target recognition algorithm based on deep learning. The faster R-CNN network discussed in this article consists of three components: 1) VGGNet [77], 2) region proposed network (RPN), and 3) fast R-CNN [78]. VGGNet is a CNN that can extract the deep features of objects. The RPN can generate target candidate regions at different scales on the feature map. Fast R-CNN combines the results of the first two modules, regresses the location of the bounding box based on the candidate regions, and determines the target type based on the scores of each category.

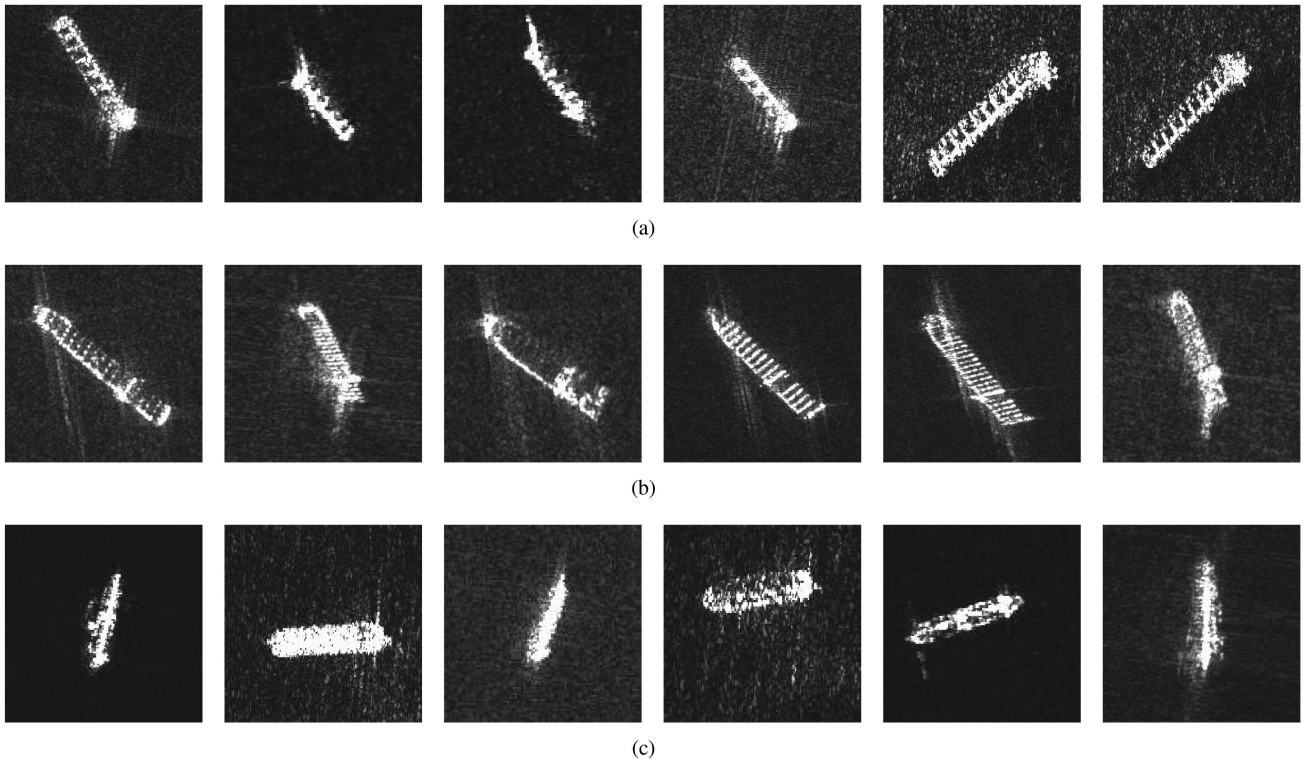

Fig. 4. Examples of SAR images of different types of ships in GPED. (a) Cargo. (b) Tanker. (c) Container.

2) SSD: The backbone of the SSD [29] algorithm is VGGNet, which serves to extract the features of the input image. The SSD algorithm removes the fully connected layer of VGGNet and obtains five extra prediction feature layers by stacking convolutional layers to achieve multiscale target recognition. The position regression of the target bounding box is achieved by setting the default box with different scales and aspect ratios on each prediction feature layer. The SSD model can be divided into SSD300 and SSD512 according to the input image size. In addition, the SSD300 model with an input image size of 300 $\times$ 300 is utilized in this article.

3) RetinaNet: The backbone of RetinaNet consists of two parts, ResNet [79] and the feature pyramid network (FPN) [80]. ResNet extracts the deep features of images using the residual module, and the FPN further processes the extracted features to accomplish feature fusion, build feature pyramids, and fully utilize the shallow network's feature information. Focal loss is proposed by RetinaNet. The focal loss adds a modulation factor to the cross-entropy loss function to mitigate the loss assigned to well classified or simple targets. Therefore, the hard examples will contribute to more loss. And this method can effectively solve the problem of the imbalanced number of samples between classes.

4) YOLOv3: The backbone of YOLOv3 [81] is Darknet53 with 53 convolutional layers and has a strong feature extraction capability by introducing a residual structure. The residual structure can reduce the risk of vanishing/exploding gradients while increasing the network depth. YOLOv3 combines convolutional operations and upsampling to fuse features of shallow and deep networks. Furthermore, this method adds two prediction feature layers to fully utilize the information in the shallow network and to enhance the detection capability of small targets. YOLOv3 draws on the experience of the anchor mechanism in faster R-CNN and sets three different scales of the anchor on each prediction feature layer to identify targets of various sizes.

5) YOLOv5: The model structure of YOLOv5 is divided into the following three parts: 1) The backbone, 2) neck, and 3) head. The backbone of YOLOv5 is cross-stage partial network Darknet53 (CSPDarknet53) [82], and the focus module is added. The neck of the YOLOv5 model is composed of FPN and PANet [83], which serves to further process the features extracted from the backbone and to improve the diversity and robustness of the features. The head of YOLOv5 constitutes a three-scale detection network through feature fusion to achieve target detection and recognition at multiple scales. The YOLOv5 algorithm is divided into the following four models according to the model size and network depth: YOLOv5s, YOLOv5m, YOLOv5l, and YOLOv5x. YOLOv5x is used in the experiments of this article.

6) EfficientDet: The backbone of EfficientDet [84] is EfficientNet [85]. EfficientNet is a CNN and is divided into seven models, which are the range of EfficientNet-B0 through EfficientNet-B6, according to the network depth and resolution of the input image. EfficientDet uses the BiFPN algorithm for feature fusion and a hybrid scaling method to scale the target detection models. Eight different model structures are obtained by the exploratory scaling method (EfficientDet-D0 to

EfficientDet-D7). We use EfficientDet-D2 for the experiments of this study.

7) PAA: Probabilistic anchor assignment (PAA) [86] is a new anchor assignment strategy. PAA first adaptively divides the anchor corresponding to each ground truth (GT) into positive samples and negative samples according to the learning state of the model. Then the anchor's score under the current model conditions is calculated and the probability distribution of anchor's score is obtained. Finally, the probability distribution is used to identify positive samples and negative samples. We constructed a target recognition model using PAA in this article. The backbone of the model is ResNet50. FPN is used for feature fusion. PAA is used to assign positive and negative sample, and focal loss is used for loss calculation.

8) VFNet: VFNet [87] (VarifocalNet) is a dense target detector. The method uses Iou-aware classification score (IACS) to express confidence and localization accuracy of the object. A new star-shaped bounding box feature representation for IACS prediction and bounding box refinement is used in the method. The backbone of the VFNet is ResNet50. FPN is used for feature fusion. The head of VFNet consists of two branches, which are used to predict the bounding box and IACS. Varifocal loss is used to train the target detector.

B. Experimental Environment and Performance Evaluation Indexes

The experiments are implemented under the PyTorch framework through the Python programming language on a 64-bit computer with Intel Xeon(R) CPU E5-2699, 128 GB RAM, and Geforce RTX2080TI with GUDA10.2 and cuDNN7.2. In order to ensure fairness, all algorithms use the uniform parameters. The initial learning rate is set to 0.001. The batch size is set to 8, and the epoch is set to 100. The stochastic gradient descent (SGD) optimizer is employed. The weight decay and momentum coefficient are set to 0.0005 and 0.9, respectively. The threshold of the intersection over union (IOU) is set to 0.5, and the threshold of confidence is set to 0.45.

The performance of the SAR ship recognition algorithm is evaluated by using the precision, recall, average precision (AP), mean average precision (mAP), and frames per second (FPS). The precision is the percentage of data that are predicted to be positive samples, and the true value of the data is also positive. The precision is used to evaluate the accuracy of the model. The recall represents the proportion of positive samples with correct predictions. The formula of precision and recall can be expressed as follows:

$$\text{precision} = \frac{TP}{TP + FP} \tag{1}$$

$$\text{recall} = \frac{TP}{TP + FN} \tag{2}$$

where true positive (TP) is the true positive that indicates the number of ships that are correctly detected, and false positive (FP) is the false positive that indicates the target number of false alarms. The parameter FN is the false negative that indicates the number of ships that miss inspection. The positive and negative samples are determined according to the IOU and confidence between the bounding box and the ground truth.

The AP is used to evaluate the accuracy of each type of ship target recognition, which is defined as the average of multiple training accuracies and is calculated as

$$AP = \int_0^1 P(R)dR \tag{3}$$

where *P* denotes precision, and *R* denotes recall.

The mAP denotes the average value of the AP for each type of ship. The mAP is an important index for evaluating the overall recognition accuracy. Moreover, FPS is used to evaluate the inference speed of the model.

IV. Generalization Performance Evaluation of the SAR Ship Recognition Method

In this section, we use eight target recognition algorithms to evaluate the generalization performance of the GPED and MTDD. These eight target recognition algorithms include faster R-CNN, SSD, YOLOv3, RetinaNet, EfficientDet, YOLOv5, PAA, and VFNet. The algorithms all use the pretraining weights on ImageNet. First, the eight algorithms are trained using the training sets of the GPED and MTDD and are tested in their respective test sets to compare the performance of the same algorithm in different datasets. Second, one dataset is selected to train the model, and the other dataset is selected for testing. This crossover experiment is utilized to evaluate the generalization performance of the GPED and MTDD.

A. Comparison of Recognition Results Between the GPED and MTDD

To evaluate the generalization performance of the GPED and MTDD, we randomly divide the GPED and MTDD into training sets, validation sets, and test sets according to a ratio of 7:2:1, respectively. We first evaluate and analyze the ship recognition accuracy of different algorithms in GPED and MTDD. The experimental results of MTDD and the GPED are shown in Tables V and VI.

Table V shows that the the average mAP of all algorithm is approximately 81.87% in MTDD. Table VI shows that the average mAP of all algorithms is approximately 64% in GPED, which is lower than that of MTDD. This result occurs because the MTDD is constructed using GF-3 satellite, which has a high ground resolution. However, GPED is constructed based on SAR images from multiple satellites, which has some low-resolution images and poor-quality images. In addition, it can be seen from Table V that the AP of container ships is lower than that of the other two types of ships, which is also the reason for the low recognition accuracy of GPED.

B. Crossover Experiment Between the GPED and MTDD

In this section, the generalization performance of the GPED and MTDD is evaluated by testing the accuracy of the ship recognition model on different datasets. The specific steps of

TABLE V
SHIP RECOGNITION RESULTS OF MTDD

Method	Backbone	AP (%)			mAP (%)
		Cargo	Tanker	Container	
Faster R-CNN	VGG16	87.80	**83.90**	**93.00**	88.23
SSD	VGG16	94.16	82.88	92.19	**89.74**
YOLOv3	DarkNet53	93.10	80.00	77.30	83.47
RetinaNet	ResNet50	95.79	81.55	66.90	81.41
EfficientDet	EfficientNet-B2	88.90	56.20	36.40	60.50
YOLOv5	CSPDarkNet53	93.30	82.80	89.20	88.43
PAA	ResNet50	**96.60**	80.80	66.20	81.20
VFNet	ResNet50	92.40	80.40	73.10	81.97

The bold entities indicates the best result for each column.

TABLE VI
SHIP RECOGNITION RESULTS OF GPED

Method	Backbone	AP (%)			mAP (%)
		Cargo	Tanker	Container	
Faster R-CNN	VGG16	76.32	76.95	54.21	69.16
SSD	VGG16	75.15	**77.69**	43.07	65.30
YOLOv3	DarkNet53	80.90	70.50	**63.10**	71.50
RetinaNet	ResNet50	73.00	74.50	46.10	64.53
EfficientDet	EfficientNet-B2	79.58	61.68	39.57	60.28
YOLOv5	CSPDarkNet53	**85.70**	66.50	62.90	**71.70**
PAA	ResNet50	66.30	66.90	38.10	57.10
VFNet	ResNet50	73.90	54.30	46.80	58.33

The bold entities indicates the best result for each column.

TABLE VII
SHIP RECOGNITION RESULTS THAT TRAINED ON GPED AND TESTED ON MTDD

Method	Backbone	AP (%)			mAP (%)
		Cargo	Tanker	Container	
Faster R-CNN	VGG16	26.77	18.13	9.53	18.14
SSD	VGG16	51.86	**34.17**	**37.73**	**41.26**
YOLOv3	DarkNet53	43.80	0.38	12.10	18.76
RetinaNet	ResNet50	32.17	7.76	15.10	18.34
EfficientDet	EfficientNet-B2	26.20	11.91	5.59	14.57
YOLOv5	CSPDarkNet53	**56.80**	31.30	18.40	35.50
PAA	ResNet50	50.80	3.90	24.10	26.26
VFNet	ResNet50	43.40	0.30	17.60	20.43

The bold entities indicates the best result for each column.

the crossover experiments are as follows. First, the ship recognition model is trained on GPED and tested on MTDD. The experimental results are shown in Table VII. Second, the ship recognition model is trained on MTDD and tested on GPED. The experimental results are shown in Table VIII.

Table VII shows that the average mAP of all algorithms is approximately 24.14%. Table VIII shows that the average mAP of all algorithms is approximately 11.26%. The ship recognition accuracy in the crossover experiments is significantly reduced because the GPED and MTDD have significant differences in terms of data sources and image resolutions, making the data distributions of the training and test sets different. This result indicates that the model trained on one dataset may not necessarily apply to another dataset and that the generalization performance of the dataset is very important for the applicability of the model. Among all the algorithms, the recognition accuracy of the GPED-based trained model is higher than that of the MTDD-based trained model, which indicates that the GPED-based trained model can be better applied to the MTDD images and proves that GPED has a better generalization performance. This result occurs because the samples in the GPED are obtained from SAR images from multiple data sources, which can better adapt to changes in the data distribution and image features in contrast to MTDD from a single data source.

Considering that the number of samples in SAR ship detection datasets is much more than that in ship recognition datasets, a novel SAR ship recognition method based on transfer learning is proposed. In this section, the principle of the proposed SAR ship recognition method is introduced, and then comparative experiments based on the GPED and MTDD are conducted to test the performance of the proposed method.

TABLE VIII
SHIP RECOGNITION RESULTS THAT TRAINED ON MTDD AND TESTED ON GPED

Method	Backbone	AP (%)			mAP (%)
		Cargo	Tanker	Container	
Faster R-CNN	VGG16	18.40	12.70	4.70	11.93
SSD	VGG16	39.14	8.34	12.79	20.09
YOLOv3	DarkNet53	13.10	2.63	2.21	5.97
RetinaNet	ResNet50	8.26	2.12	1.92	4.10
EfficientDet	EfficientNet-B2	21.60	1.70	7.50	10.27
YOLOv5	CSPDarkNet53	**49.4**	**13.90**	**34.00**	**32.43**
PAA	ResNet50	3.70	0.90	0.70	1.77
VFNet	ResNet50	6.30	2.20	2.10	3.53

The bold entities indicates the best result for each column.

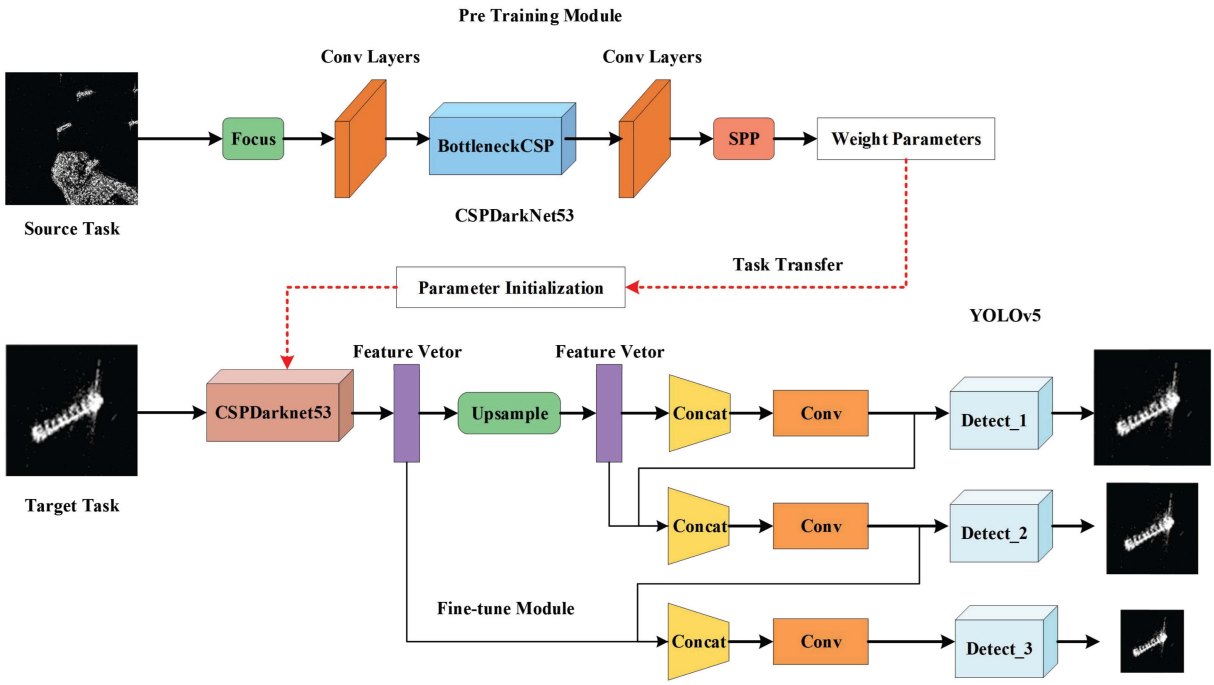

Fig. 5. General framework of the ship recognition method based on the task transfer.

C. Proposed Method

The basic idea of transfer learning is to transfer information from the source domain to the target domain. The source domain and target domain are usually different domains; thus, transfer learning is essentially a cross-domain data migration. The method of cross-domain migration imposes strict requirements on the similarity between the source domain and the target domain. When the data distribution of the source domain and the target domain significantly differs, domain mismatch and even negative migration may occur [88]. Therefore, we proposed an SAR ship recognition method based on task transfer, which transfers migration learning from different domains to the same domain (SAR domain) without considering the similarity between the source domain and the target domain. The source task in the proposed method is SAR ship detection, and the target task is SAR ship recognition. The specific steps of this method are as follows. First, the model is trained using the SAR ship detection dataset and saves the weight parameters of the model. Second, the target model is initialized by using the weight parameters. Last, the whole model will be fine-tuned based on the SAR ship recognition dataset. The method is equivalent to merging the data in the source domain and target domain, which can somewhat improve the generalization performance of the model. Both the source domain and target domain in this method are SAR image domains, which eliminates the influence of the differences in the data distribution on transfer learning. The framework of the SAR ship recognition method based on task transfer is shown in Fig. 5, which is divided into the following two modules: 1) The pretraining module and 2) the fine-tuning module.

1) Pretraining Module: Most target recognition algorithms based on deep learning are divided into the following two parts: 1) Feature extraction and 2) classification. As the first step of target recognition, feature extraction has a very important role in the target recognition model. The pretraining module is applied to the feature extraction part of the SAR ship recognition

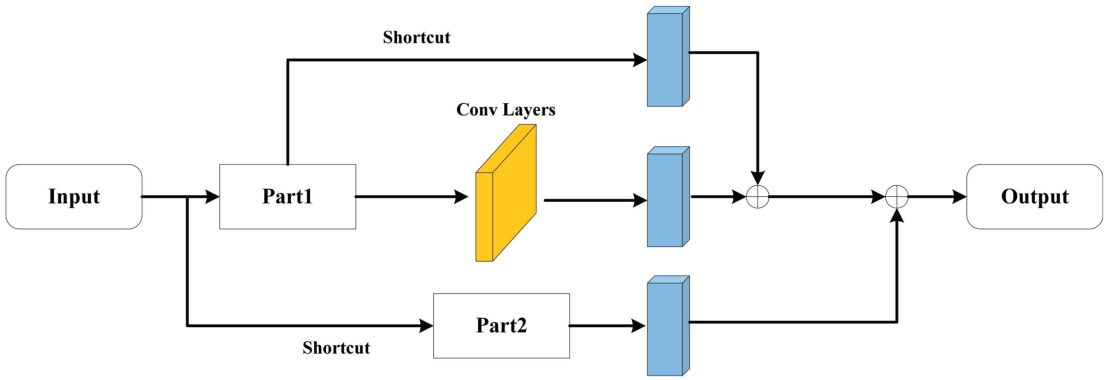

Fig. 6. Basic structure of the pretraining module.

model. Pretraining means that the feature extraction network of the target task model is trained in the source task so that the model of the target task is trained with a better initial parameter instead of with random parameters. These parameters contain some general feature information of the ship target, such as the length, width, area, and texture of the ship. These features can distinguish the ship from the background. As a result, they are not only useful in ship detection tasks but also effective in ship recognition tasks.

The feature extraction of images in target recognition usually employs CNN algorithms, such as VGGNet, ResNet, and Darknet53, with excellent performance. Although these networks can extract deep features of images, there is a large amount of repetitive gradient learning during the training process, which increases the computational effort and reduces the learning ability of the model. To reduce repetitive gradient learning, CSPNet is proposed and introduced into the CNN. CSPNet decreases the gradient variability by integrating feature maps at the beginning and end of the network stages. CSPNet is introduced into the Darknet53 network to form CSPDarknet53, which is the basis of the pretraining module in this section. Fig. 6 shows the basic structure of the pretraining module. A new residual module is added to the original residual module, and the feature maps obtained from Part 2 are further fused with those processed by Part 1 and multiple residual blocks to achieve a richer combination of gradients. The network is trained using the labeled samples from the source task to obtain the trained CSPDarknet53 model, i.e., the pretrained model.

2) Fine-Tuning Module: After pretraining the feature extraction network for the SAR ship recognition model, we obtain the initialized feature extraction network CSPDarknet53. The network can extract features that distinguish ships from other targets, but the model still needs to be further trained using the dataset of the target task to extract detailed information about the ship targets, and thus, classify the specific types of ships. Therefore, we use SAR ship recognition datasets to fine-tune the CSPDarknet53 and YOLOv5 classifiers. The reason why we used YOLOv5 as the benchmark is that YOLOv5 is the state-of-the-art method on GPED dataset in Table VI. First, the loss obtained from forwarding propagation of the model is calculated, and second, the error is backpropagated using stochastic gradient descent to update the weight parameters of the whole network. The loss of this process consists of the following three parts: 1) Localization loss, 2) confidence loss, and 3) classification loss. The confidence loss $\text{Loss}_{\text{conf}}$ and class loss $\text{Loss}_{\text{class}}$ are calculated as follows:

$$\begin{aligned}\text{Loss}_{\text{conf}} = &-\sum_{i=0}^{K\times K} I_{ij}^{\text{obj}}\left[\hat{c}_i \log c_i^j + \left(1-\hat{c}_i^j\right)\log\left(1-c_i^j\right)\right] \\ &-\lambda_{\text{noobj}}\sum_{i=0}^{K\times K}\sum_{j=0}^{M} I_{ij}^{\text{noobj}}\left[\hat{c}_i^j \log c_i^j \right. \\ &\left.+\left(1-\hat{c}_i^j\right)\log\left(1-c_i^j\right)\right] \qquad (4)\end{aligned}$$

$$\begin{aligned}\text{Loss}_{\text{class}} = &-\sum_{i=0}^{K\times K} I_{ij}^{\text{obj}} \sum_{c\in \text{classes}}\left[\widehat{P}_i^j \log P_i^j \right. \\ &\left.+\left(1-\widehat{P}_i^j\right)\log\left(1-P_i^j\right)\right] \qquad (5)\end{aligned}$$

where K denotes the final feature map divided into $K \times K$ grids, and M denotes the number of anchors that correspond to each grid. The term I_{ij}^{noobj} denotes the anchors without targets, and λ_{noobj} is the weight factor.

Localization loss refers to the error between the position of the target bounding box that is predicted by the ship recognition model and the ground truth box. In the ship recognition task, rectangular boxes are usually employed to localize the target, which provides the feasibility of calculating the minimum enclosing area of the target. Therefore, the IOU is usually applied to calculate the localization loss. The IOU reflects the overlap between the bounding box and ground truth boxes, and the IOU of A and B is defined as

$$\text{IOU} = \frac{A \cap B}{A \cup B}. \qquad (6)$$

The IOU has scale invariance, and the similarity between any bounding boxes and the ground truth is independent of

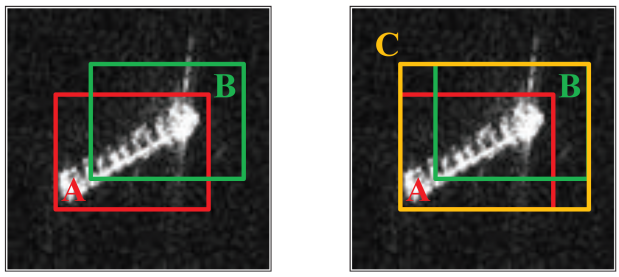

Fig. 7. Relationship of the bounding box between IOU and GIOU. (a) IOU. (b) GIOU.

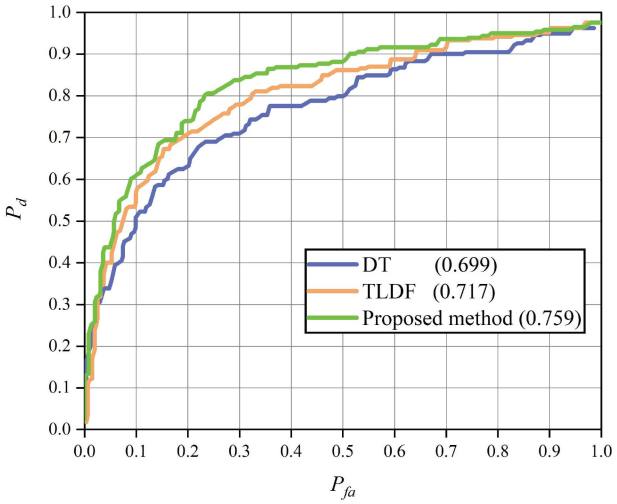

Fig. 8. ROC curves of the different methods on GPED.

their spatial scale size. Only the overlap degree between the bounding box and the ground truth is selected for measurement. According to the formula, the IOU is zero when the bounding box and ground truth do not intersect. In this case, the IOU cannot reflect the distance between the two bounding boxes, and thus, the location error between the bounding box and the ground truth cannot be determined. In addition, distinguishing different alignments between two objects by using the IOU is impossible, i.e., the IOU of two overlapping objects with the same intersection level in different directions will be equal. To solve the above problems, we use a generalized IOU (GIOU) [89] to calculate the localization loss. Fig. 7 shows the bounding box relationship between the IOU and the GIOU. The GIOU considers the nonoverlapping regions that do not belong to A and B, and the minimum enclosing rectangle (C) of the two targets is involved in the calculation to effectively respond to the overlapping way of A and B. Thus, the result of the localization loss is more stable. The GIOU is defined as

$$\mathrm{GIOU} = \mathrm{IOU} - \frac{C - (A \cup B)}{C}. \tag{7}$$

TABLE IX
EXPERIMENTAL RESULTS OF DIFFERENT METHODS ON GPED

Method	AP (%)			mAP (%)	FPS
	Cargo	Tanker	Container		
DT	84.80	71.00	53.90	69.90	27.41
FT	75.30	72.50	44.50	64.10	20.52
TLDF	85.70	66.50	**62.90**	71.70	**27.84**
Proposed Method	**86.30**	**79.20**	62.20	**75.90**	27.76

The bold entities indicates the best result for each column.

TABLE X
EXPERIMENTAL RESULTS OF DIFFERENT METHODS ON MTDD

Method	AP (%)			mAP (%)	FPS
	Cargo	Tanker	Container		
DT	94.50	86.10	82.40	87.70	23.01
FT	86.50	39.60	31.30	52.40	22.14
TLDF	93.30	82.80	89.20	88.50	**23.26**
Proposed Method	**97.40**	**86.80**	**90.90**	**91.70**	19.76

The bold entities indicates the best result for each column.

Based on the GIOU, the final target localization loss $\mathrm{Loss}_{\mathrm{loc}}$ is obtained

$$\mathrm{Loss}_{\mathrm{loc}} = 1 - \mathrm{GIOU} = 1 - \mathrm{IOU} + \frac{C - (A \cup B)}{C}. \tag{8}$$

Through the calculation of the above three losses, the loss of the SAR ship recognition algorithm is obtained. The total loss is assigned according to the backpropagation principle, and the parameters of each layer are updated by using the SGD optimization function.

D. Experimental Results and Analysis

According to the experimental settings and evaluation metrics in Section III, we conducted experiments based on the SAR-ship-dataset, MTDD, and GPED. SAR-ship-dataset is a large-scale SAR ship detection dataset for complex scenes. This dataset is publicly available in [39] and contains 43 819 labeled samples. The dataset can meet our experimental needs. According to the SAR ship recognition method proposed in this article, first, the model is trained using the SAR-ship-dataset. Second, the model is fine-tuned using the training set of GPED (MTDD). Last, the performance of the proposed method is tested using the test set of GPED (MTDD). To make the results more intuitive, experiments are conducted by using the following two methods to compare the experimental results: 1) Direct training (DT): No transfer learning method is used, and the model is trained using the initial parameters; 2) freeze training (FT): Backbone of the model is frozen during training and the parameters are not updated; 3) transfer learning from different domains (TLDF): The natural image domain (ImageNet) is selected as the source domain for cross-domain knowledge transfer [65]. The results are shown in Tables IX and X.

Tables IX and X show that the proposed method has the highest recognition accuracy. The mAP of the proposed method

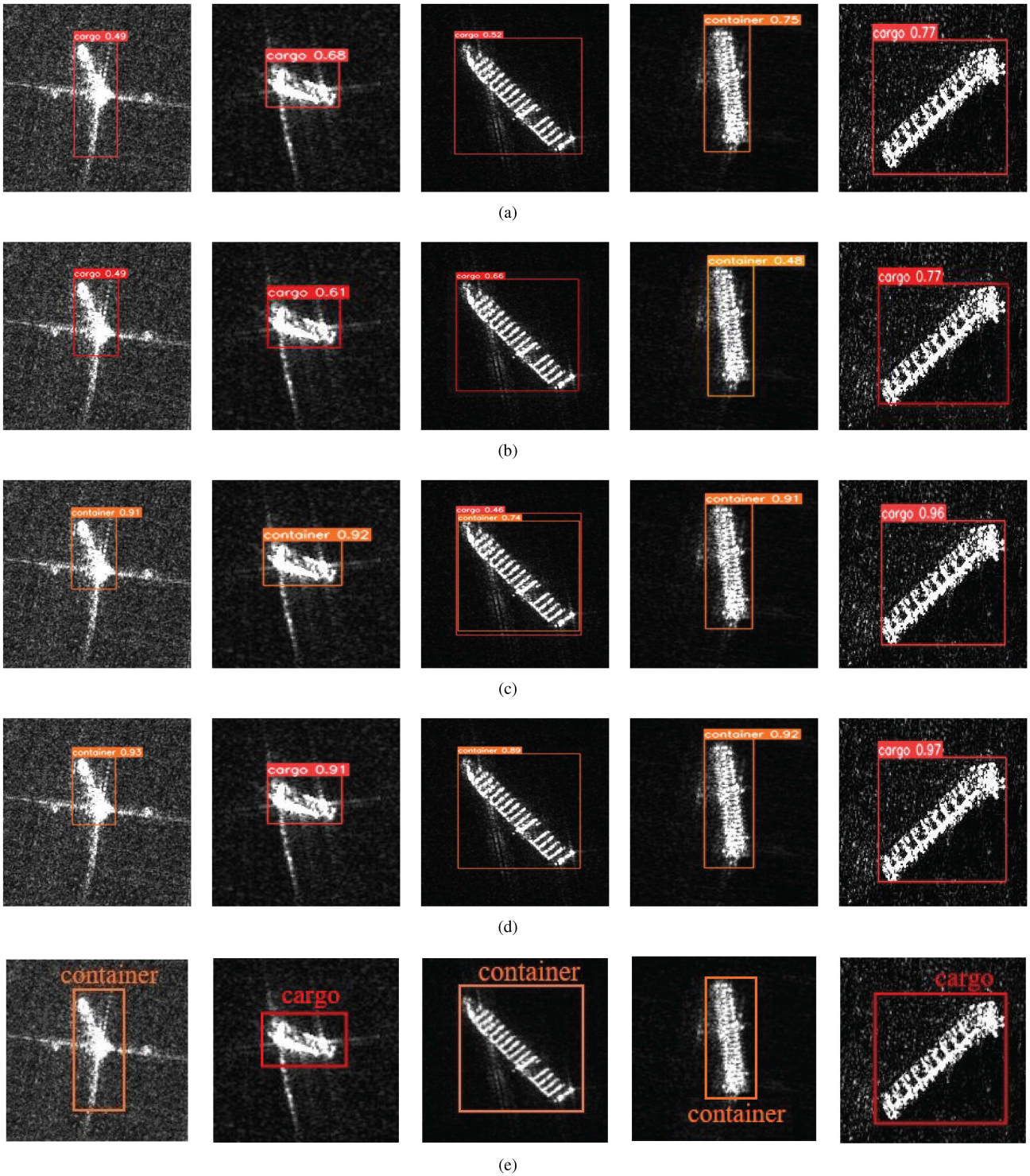

Fig. 9. Comparison of ship recognition results of different methods. (a) DT. (b) FT. (c) TLDF. (d) Proposed method. (e) Ground truth.

on GPED and MTDD is 75.9% and 91.7%, respectively. The results indicate that our method can effectively achieve knowledge migration from the ship detection task to the ship recognition task. Because the data distribution of training set and test set in MTDD is more similar than that in GPED, the mAP achieved by the proposed method on GPED is about 15% lower than the one obtained on MTDD. Thus, the proposed method is proven to be superior to the cross-domain migration method because our method is performed in the SAR image domain, which avoids the performance degradation caused by the differences in the data distribution and image features of different domains. In addition, the mAP of our method on GPED and MTDD is higher than that of the method without transfer learning, which indicates that transfer learning is beneficial to ship recognition

TABLE XI
EXPERIMENTAL RESULTS OF DIFFERENT METHODS TRAINED ON GPED AND TESTED ON MTDD

Method	AP (%)			mAP (%)	FPS
	Cargo	Tanker	Container		
DT	61.80	25.00	13.00	33.30	17.99
FT	63.50	21.70	17.60	34.30	**22.28**
TLDF	56.80	31.30	**18.40**	35.50	20.81
Proposed Method	**63.50**	**36.10**	13.00	**37.50**	18.84

The bold entities indicates the best result for each column.

TABLE XII
EXPERIMENTAL RESULTS OF DIFFERENT METHODS TRAINED ON MTDD AND TESTED ON GPED

Method	AP (%)			mAP (%)	FPS
	Cargo	Tanker	Container		
DT	46.60	17.50	21.40	28.50	23.64
FT	21.50	9.49	8.32	13.10	25.54
TLDF	49.40	13.90	**34.00**	32.40	**25.76**
Proposed Method	**52.50**	**25.60**	33.10	**37.00**	24.94

The bold entities indicates the best result for each column.

in SAR images. The mAP of our method on GPED and MTDD is higher than that of the freeze training method, which further proves the advantages of the proposed method. Among the three types of ships, the recognition accuracy of cargo ships and tankers is improved, and the recognition accuracy of container ships does not change much on GPED, which indicates that our method applies to different types of ships. Moreover, the results of FPS show that the inference speed of the proposed method is slightly lower than that of TLDF method, which means that the computational of the proposed method has slightly increased.

To further evaluate the performance of the proposed method, we performed cross experiments between GPED and MTDD. Tables XI and XII show the ship recognition accuracy of the models trained on GPED and MTDD, respectively. The experimental results show that the accuracy of the proposed method is higher than that of other methods, which proves the effectiveness of the proposed method. Moreover, the accuracy of the model trained on GPED is higher than that of the model trained on MTDD, which further proves that GPED has better generalization performance.

Positive and negative samples of ship recognition are obtained according to the threshold of GIOU and confidence. We define the recognition rate P_d as the proportion of samples that are predicted to be positive in all positive samples and define the false alarm P_{fa} as the proportion of samples that are predicted to be positive in all negative samples. The receiver operating characteristic (ROC) curves of the different methods on GPED are shown in Fig. 8. One can see that the proposed method has a higher recognition rate than other methods at a constant false alarm rate. The method also has a lower false alarm rate than other methods at a constant recognition ratio. In addition, the recognition results of the different methods in test samples are shown in Fig. 9, which prove that the recognition performance of the proposed method is better than that of the other methods.

V. CONCLUSION

The active recognition of ship targets has been getting refined with the development of deep learning. However, most of the published ship recognition datasets use a single SAR satellite sensor. It needs to be evaluated and analyzed carefully whether the model trained by a single satellite dataset can still achieve the same accuracy with different SAR satellites. In this article, an SAR ship recognition dataset is constructed based on SAR images from multiple SAR satellites and is named the GPED. Then we evaluate and analyze the generalization performance of current mainstream deep learning methods on the GPED and MTDD. The experimental results show that the GPED has a better generalization performance than MTDD. Moreover, considering that the number of samples in SAR ship detection datasets is much more than that in ship recognition datasets, an SAR ship recognition method based on task transfer is proposed in this article. The proposed method can apply ship samples with unlabeled type to ship recognition, thereby realizing knowledge transfer from ship detection tasks to ship recognition tasks. The experimental results on the GPED and MTDD show that the mAP of the proposed method is 75.9% and 91.7%, respectively, which achieves state-of-the-art performance. The method has great potential in the application of an SAR ship recognition system. However, the inference speed of the proposed method is slightly reduced and the pretraining module of the method will take a long time. In addition, due to the uneven distribution of the incident angle of the images in the dataset, we did not consider the impact of the change of the incident angle on the SAR ship recognition accuracy. In the future, we will focus on this topic.

ACKNOWLEDGMENT

The authors would like to thank the National Satellite Ocean Application Service of China, DLR (Deutsches Zentrum für Luftund Raumfahrt), the Canadian Space Agency (CSA), and Application and Copernicus Open Access Hub for providing Gaofen-3 images, TerraSAR-X images, RADARSAT-2 images, and Sentinel-1 images, respectively. The authors would also like to thank Associate Professor Wei Yang from Beihang University for sharing the MTDD generously.

The authors would like to thank American Journal Experts (AJE) for their professional English language editing services.

REFERENCES

[1] H. Lang, Y. Xi, and X. Zhang, "Ship detection in high-resolution SAR images by clustering spatially enhanced pixel descriptor," *IEEE Trans. Geosci. Remote Sens.*, vol. 57, no. 8, pp. 5407–5423, Aug. 2019.

[2] R. Yang, Z. Pan, X. Jia, L. Zhang, and Y. Deng, "A novel CNN-based detector for ship detection based on rotatable bounding box in SAR images," *IEEE J. Sel. Topics Appl. Earth Observ. Remote Sens.*, vol. 14, pp. 1938–1958, 2021.

[3] T. Liu, J. Zhang, G. Gao, J. Yang, and A. Marino, "CFAR ship detection in polarimetric synthetic aperture radar images based on whitening filter," *IEEE Trans. Geosci. Remote Sens.*, vol. 58, no. 1, pp. 58–81, Jan. 2019.

[4] G. W. Liu, J. Zhang, X. Zhang, and G. Y. Wang, "Applicability analysis of clutter model in ship detection with different resolution SAR images," *J. Ocean Univ. China, Nat. Sci.*, vol. 47, no. 2, pp. 70–78, 2017.

[5] G. V. Trunk, "Range resolution of targets using automatic detectors," *IEEE Trans. Aerosp. Electron. Syst.*, vol. AES-14, no. 5, pp. 750–755, Sep. 1978.

[6] M. E. Smith and P. K. Varshney, "Intelligent CFAR processor based on data variability," *IEEE Trans. Aerosp. Electron. Syst.*, vol. 36, no. 3, pp. 837–847, Jul. 2000.

[7] H. Rohling, "Radar CFAR thresholding in clutter and multiple target situations," *IEEE Trans. Aerosp. Electron. Syst.*, vol. AES-19, no. 4, pp. 608–621, Jul. 1983.

[8] P. P. Gandhi and S. A. Kassam, "Analysis of CFAR processors in non-homogeneous background," *IEEE Trans. Aerosp. Electron. Syst.*, vol. 24, no. 4, pp. 427–445, Jul. 1988.

[9] G. Margarit and A. Tabasco, "Ship classification in single-pol SAR images based on fuzzy logic," *IEEE Trans. Geosci. Remote Sens.*, vol. 49, no. 8, pp. 3129–3138, Aug. 2011.

[10] H. Zhang, X. Tian, C. Wang, F. Wu, and B. Zhang, "Merchant vessel classification based on scattering component analysis for COSMO-SkyMed SAR images," *IEEE Geosci. Remote Sens. Lett.*, vol. 10, no. 6, pp. 1275–1279, Nov. 2013.

[11] H. Lang and S. Wu, "Ship classification in moderate-resolution SAR image by naive geometric features-combined multiple kernel learning," *IEEE Geosci. Remote Sens. Lett.*, vol. 14, no. 10, pp. 1765–1769, Oct. 2017.

[12] H. Lang, J. Zhang, X. Zhang, and J. Meng, "Ship classification in SAR image by joint feature and classifier selection," *IEEE Geosci. Remote Sens. Lett.*, vol. 13, no. 2, pp. 212–216, Feb. 2015.

[13] J. C. Ni, Q. Zhang, Q. Yang, Y. Luo, and L. Sun, "Directional feature: A novel feature for group target detection in high resolution SAR images," *Remote Sens. Lett.*, vol. 8, no. 7/9, pp. 713–722, 2017.

[14] X. Zhang, J. Zhang, J. I. Yong-Gang, and J. M. Meng, "The capability analysis of ship classification by structure feature using SAR images," *Acta Oceanol. Sin.*, vol. 32, no. 01, pp. 146–152, 2010.

[15] R. L. Paes, F. Nunziata, and M. Migliaccio, "On the capability of hybrid-polarity features to observe metallic targets at sea," *IEEE J. Ocean. Eng.*, vol. 41, no. 2, pp. 346–361, Apr. 2016.

[16] G. Margarit, J. J. Mallorqui, and X. Fabregas, "Single-pass polarimetric SAR interferometry for vessel classification," *IEEE Trans. Geosci. Remote Sens.*, vol. 45, no. 11, pp. 3494–3502, Nov. 2007.

[17] G. Margarit, J. J. Mallorqui, J. Fortuny-Guasch, and C. Lopez-Martinez, "Exploitation of ship scattering in polarimetric SAR for an improved classification under high clutter conditions," *IEEE Trans. Geosci. Remote Sens.*, vol. 47, no. 4, pp. 1224–1235, Apr. 2009.

[18] M. Sato, X. S. Wang, and S. W. Chen, "Uniform polarimetric matrix rotation theory and its applications," *IEEE Trans. Geosci. Remote Sens.*, vol. 52, no. 8, pp. 4756–4770, Aug. 2014.

[19] S. W. Chen, "Polarimetric coherence pattern: A visualization and characterization tool for PolSAR data investigation," *IEEE Trans. Geosci. Remote Sens.*, vol. 56, no. 1, pp. 286–297, Jan. 2018.

[20] M. Migliaccio, F. Nunziata, A. Montuori, and C. Brown, "Marine added-value products using Radarsat-2 fine quad-polarization," *Can. J. Remote Sens.*, vol. 37, no. 5, pp. 443–451, 2011.

[21] S. W. Chen, X. C. Cui, X. S. Wang, and S. P. Xiao, "Speckle-free SAR image ship detection," *IEEE Trans. Image Process.*, vol. 30, pp. 5969–5983, 2021.

[22] H. Lang, J. Zhang, T. Zhang, D. Zhao, and J. Meng, "Hierarchical ship detection and recognition with high-resolution polarimetric synthetic aperture radar imagery," *J. Appl. Remote Sens.*, vol. 8, no. 1, 2014, Art. no. 083623.

[23] C. Wang, H. Zhang, F. Wu, and S. Jiang, "A novel hierarchical ship classifier for cosmo-skymed SAR data," *IEEE Geosci. Remote Sens. Lett.*, vol. 11, no. 2, pp. 484–488, Feb. 2014.

[24] J. Zhu, X. Qiu, Z. Pan, Y. Zhang, and B. Lei, "Projection shape template-based ship target recognition in TerraSAR-X images," *IEEE Geosci. Remote Sens. Lett.*, vol. 14, no. 2, pp. 222–226, Feb. 2017.

[25] M. Amrani, F. Jiang, Y. Xu, S. Liu, and S. Zhang, "SAR-oriented visual saliency model and directed acyclic graph support vector metric based target classification," *IEEE J. Sel. Topics Appl. Earth Observ. Remote Sens.*, vol. 11, no. 10, pp. 3794–3810, Oct. 2018.

[26] M. Amrani, K. Yang, D. Zhao, X. Fan, and F. Jiang, "An efficient feature selection for SAR target classification," in *Proc. Pacific Rim Conf. Multimedia*, 2017, pp. 68–78.

[27] M. Amrani, S. Chaib, I. Omara, and F. Jiang, "Bag-of-visual-words based feature extraction for SAR target classification," in *Proc. 9th Int. Conf. Digit. Image Process.*, 2017, vol. 10420, pp. 327–332.

[28] S. Ren, K. He, R. Girshick, and J. Sun, "Faster R-CNN: Towards real-time object detection with region proposal networks," *IEEE Trans. Pattern Anal. Mach. Intell.*, vol. 39, no. 6, pp. 1137–1149, Jun. 2017.

[29] W. Liu et al., "SSD: Single shot multibox detector," in *Proc. Eur. Conf. Comput. Vision*, 2016, pp. 21–37.

[30] J. Redmon, S. Divvala, R. Girshick, and A. Farhadi, "You only look once: Unified, real-time object detection," in *Proc. IEEE Conf. Comput. Vis. Pattern Recognit.*, 2016, pp. 779–788.

[31] T.-Y. Lin, P. Goyal, R. Girshick, K. He, and P. Dollár, "Focal loss for dense object detection," *IEEE Trans. Pattern Anal. Mach. Intell.*, vol. 42, no. 2, pp. 318–327, Feb. 2020.

[32] H. Law and J. Deng, "Cornernet: Detecting objects as paired keypoints," in *Proc. Eur. Conf. Comput. Vis.*, 2018, pp. 734–750.

[33] K. Duan, S. Bai, L. Xie, H. Qi, Q. Huang, and Q. Tian, "Centernet: Keypoint triplets for object detection," in *Proc. IEEE Int. Conf. Comput. Vis.*, 2019, pp. 6569–6578.

[34] Z. Tian, C. Shen, H. Chen, and T. He, "FCOS: Fully convolutional one-stage object detection," in *Proc. IEEE Int. Conf. Comput. Vis.*, 2019, pp. 9627–9636.

[35] T. Kong, F. Sun, H. Liu, Y. Jiang, L. Li, and J. Shi, "FoveaBox: Beyound anchor-based object detection," *IEEE Trans. Image Process.*, vol. 29, pp. 7389–7398, 2020.

[36] N. Carion, F. Massa, G. Synnaeve, N. Usunier, A. Kirillov, and S. Zagoruyko, "End-to-end object detection with transformers," in *Proc. Eur. Conf. Comput. Vision*, 2020, pp. 213–229.

[37] A. Dosovitskiy et al., "An image is worth 16×16 words: Transformers for image recognition at scale," 2020, *arXiv:2010.11929*.

[38] J. Li, C. Qu, and J. Shao, "Ship detection in SAR images based on an improved faster R-CNN," in *Proc. SAR Big Data Era, Models, Methods Appl.*, 2017, pp. 1–6.

[39] Y. Wang, C. Wang, H. Zhang, Y. Dong, and S. Wei, "A SAR dataset of ship detection for deep learning under complex backgrounds," *Remote Sens.*, vol. 11, no. 7, 2019, Art. no. 765.

[40] X. Sun, Z. R. Wang, Y. R. Sun, W. H. Diao, Y. Zhang, and K. Fu, "AIR-SARship-1.0: High-resolution SAR ship detection dataset," *J. Radars*, vol. 8, no. 6, pp. 852–862, 2019.

[41] S. J. Wei, X. F. Zeng, Q. Z. Qu, M. Wang, H. Su, and J. Shi, "Hrsid: A high-resolution SAR images dataset for ship detection and instance segmentation," *IEEE Access*, vol. 8, pp. 120234–120254, 2020.

[42] T. Zhang, X. Zhang, X. Ke, X. Zhan, and D. Kumar, "LS-SSDD-V1.0: A deep learning dataset dedicated to small ship detection from large-scale sentinel-1 SAR images," *Remote Sens.*, vol. 12, no. 18, 2020, Art. no. 2997.

[43] M. Kang, K. Ji, X. Leng, and Z. Lin, "Contextual region-based convolutional neural network with multilayer fusion for SAR ship detection," *Remote Sens.*, vol. 9, no. 8, 2017, Art. no. 860.

[44] X. Zhang et al., "A lightweight feature optimizing network for ship detection in SAR image," *IEEE Access*, vol. 7, pp. 141662–141678, 2019.

[45] Z. Lin, K. Ji, X. Leng, and G. Kuang, "Squeeze and excitation rank faster R-CNN for ship detection in SAR images," *IEEE Geosci. Remote Sens. Lett.*, vol. 16, no. 5, pp. 751–755, May 2019.

[46] Y. L. Chang, A. Anagaw, L. Chang, Y. C. Wang, C.-Y. Hsiao, and W.-H. Lee, "Ship detection based on YOLOv2 for SAR imagery," *Remote Sens.*, vol. 11, no. 7, 2019, Art. no. 786.

[47] J. Redmon and A. Farhadi, "YOLO9000: Better, faster, stronger," in *Proc. IEEE Conf. Comput. Vis. Pattern Recognit.*, 2017, pp. 7263–7271.

[48] Y. Wang, C. Wang, H. Zhang, Y. Dong, and S. Wei, "Automatic ship detection based on retinanet using multi-resolution Gaofen-3 imagery," *Remote Sens.*, vol. 11, no. 5, 2019, Art. no. 531.

[49] Z. Hou, Z. Cui, Z. Cao, and N. Liu, "An integrated method of ship detection and recognition in SAR images based on deep learning," in *Proc. IEEE Int. Geosci. Remote Sens. Symp.*, 2020, pp. 1225–1228.

[50] G. Tang, Y. Zhuge, C. Claramunt, and S. Men, "N-YOLO: A SAR ship detection using noise-classifying and complete-target extraction," *Remote Sens.*, vol. 13, no. 5, 2021, Art. no. 871.

[51] Y. Hu, Y. Li, and Z. Pan, "A dual-polarimetric SAR ship detection dataset and a memory-augmented autoencoder-based detection method," *Sensors*, vol. 21, no. 24, 2021, Art. no. 8478.

[52] M. Amrani, M. Hammad, F. Jiang, K. Wang, and A. Amrani, "Very deep feature extraction and fusion for arrhythmias detection," *Neural. Comput. Appl.*, vol. 30, no. 7, pp. 2047–2057, 2018.

[53] X. Xing, K. Ji, H. Zou, W. Chen, and J. Sun, "Ship classification in TerraSAR-X images with feature space based sparse representation," *IEEE Geosci. Remote Sens. Lett.*, vol. 10, no. 6, pp. 1562–1566, Nov. 2013.
[54] L. Huang et al., "OpenSARShip: A dataset dedicated to sentinel-1 ship interpretation," *IEEE J. Sel. Topics Appl. Earth Observ. Remote Sens.*, vol. 11, no. 1, pp. 195–208, Jan. 2018.
[55] J. He, Y. Wang, and H. Liu, "Ship classification in medium-resolution SAR images via densely connected triplet CNNs integrating fisher discrimination regularized metric learning," *IEEE Trans. Geosci. Remote Sens.*, vol. 59, no. 4, pp. 3022–3039, Apr. 2021.
[56] M. Ma, J. Chen, W. Liu, and W. Yang, "Ship classification and detection based on CNN using GF-3 SAR images," *Remote Sens.*, vol. 10, no. 12, 2018, Art. no. 2043.
[57] X. Hou, W. Ao, Q. Song, J. Lai, H. Wang, and F. Xu, "FUSAR-ship: Building a high-resolution SAR-AIS matchup dataset of Gaofen-3 for ship detection and recognition," *Sci. China Inf. Sci.*, vol. 63, no. 4, 2020, Art. no. 140303.
[58] S. Lei, D. Lu, X. Qiu, and C. Ding, "SRSDD-V1. 0: A high-resolution SAR rotation ship detection dataset," *Remote Sens.*, vol. 13, no. 24, 2021, Art. no. 5104.
[59] T. Zhang and X. Zhang, "A polarization fusion network with geometric feature embedding for SAR ship classification," *Pattern Recognit.*, vol. 123, 2022, Art. no. 108365.
[60] M. Amrani, A. Bey, and A. Amamra, "New SAR target recognition based on YOLO and very deep multi-canonical correlation analysis," *Int. J. Remote Sens.*, pp. 1–20, 2021.
[61] M. Amrani and F. Jiang, "Deep feature extraction and combination for synthetic aperture radar target classification," *J. Appl. Remote Sens.*, vol. 11, no. 4, 2017, Art. no. 042616.
[62] S. W. Chen, X. S. Wang, and M. Sato, "PolinSAR complex coherence estimation based on covariance matrix similarity test," *IEEE Geosci. Remote Sens. Lett.*, vol. 50, no. 11, pp. 4699–4710, Nov. 2012.
[63] S. W. Chen, "SAR image speckle filtering with context covariance matrix formulation and similarity test," *IEEE Trans. Image Process.*, vol. 29, pp. 6641–6654, 2020.
[64] J. Deng, W. Dong, R. Socher, L.-J. Li, K. Li, and L. Fei-Fei, "ImageNet: A large-scale hierarchical image database," in *Proc. IEEE Conf. Comput. Vis. Pattern Recognit.*, 2009, pp. 248–255.
[65] Y. Wang, C. Wang, and H. Zhang, "Combining a single shot multibox detector with transfer learning for ship detection using sentinel-1 SAR images," *Remote Sens. Lett.*, vol. 9, no. 8, pp. 780–788, 2018.
[66] M. Rostami, S. Kolouri, E. Eaton, and K. Kim, "Deep transfer learning for few-shot SAR image classification," *Remote Sens.*, vol. 11, no. 11, 2019, Art. no. 1374.
[67] Z. Huang, Z. Pan, and B. Lei, "What, where, and how to transfer in SAR target recognition based on deep CNNs," *IEEE Trans. Geosci. Remote Sens.*, vol. 58, no. 4, pp. 2324–2336, Apr. 2019.
[68] M. D. Graziano, M. D'Errico, and E. Razzano, "Constellation analysis of an integrated AIS/remote sensing spaceborne system for ship detection," *Adv. Space Res.*, vol. 50, no. 3, pp. 351–362, 2012.
[69] Y. Xu and H. Lang, "Ship classification in SAR images with geometric transfer metric learning," *IEEE Trans. Geosci. Remote Sens.*, vol. 59, no. 8, pp. 6799–6813, Aug. 2021.
[70] Y. Xu, H. Lang, L. Niu, and C. Ge, "Discriminative adaptation regularization framework-based transfer learning for ship classification in SAR images," *IEEE Geosci. Remote Sens. Lett.*, vol. 16, no. 11, pp. 1786–1790, Nov. 2019.
[71] H. Lang, S. Wu, and Y. Xu, "Ship classification in SAR images improved by AIS knowledge transfer," *IEEE Geosci. Remote Sens. Lett.*, vol. 15, no. 3, pp. 439–443, Mar. 2018.
[72] M. Rodger and R. Guida, "Classification-aided SAR and AIS data fusion for space-based maritime surveillance," *Remote Sens.*, vol. 13, no. 1, 2020, Art. no. 104.
[73] Y. Shi, L. Du, and Y. Guo, "Unsupervised domain adaptation for SAR target detection," *IEEE J. Sel. Topics Appl. Earth Observ. Remote Sens.*, vol. 14, pp. 6372–6385, 2021.
[74] T. Lin, "Labelimg," 2015. [Online]. Available: https://github. com/tzutalin/labelImg
[75] T. Zhang et al., "Balance learning for ship detection from synthetic aperture radar remote sensing imagery," *ISPRS J. Photogramm. Remote Sens.*, vol. 182, pp. 190–207, 2021.
[76] S. W. Chen, X. S. Wang, S. P. Xiao, and M. Sato, *Target Scattering Mechanism in Polarimetric Synthetic Aperture Radar: Interpretation and Application*. Berlin, Germany: Springer, 2018.
[77] K. Simonyan and A. Zisserman, "Very deep convolutional networks for large-scale image recognition," 2014, *arXiv:1409.1556*.
[78] R. Girshick, "Fast R-CNN," in *Proc. IEEE Conf. Comput. Vis. Pattern Recognit.*, 2015, pp. 1440–1448.
[79] K. He, X. Zhang, S. Ren, and J. Sun, "Deep residual learning for image recognition," in *Proc. IEEE Conf. Comput. Vis. Pattern Recognit.*, 2016, pp. 770–778.
[80] T.-Y. Lin, P. Dollár, R. Girshick, K. He, B. Hariharan, and S. Belongie, "Feature pyramid networks for object detection," in *Proc. IEEE Conf. Comput. Vis. Pattern Recognit.*, 2017, pp. 2117–2125.
[81] J. Redmon and A. Farhadi, "YOLOV3: An incremental improvement," 2018, *arXiv:1804.02767*.
[82] C.-Y. Wang, H.-Y. M. Liao, Y.-H. Wu, P.-Y. Chen, J.-W. Hsieh, and I.-H. Yeh, "CSPNet: A new backbone that can enhance learning capability of CNN," in *Proc. IEEE Conf. Comput. Vis. Pattern Recognit.*, 2020, pp. 390–391.
[83] S. Liu, L. Qi, H. Qin, J. Shi, and J. Jia, "Path aggregation network for instance segmentation," in *Proc. IEEE Conf. Comput. Vis. Pattern Recognit.*, 2018, pp. 8759–8768.
[84] M. Tan, R. Pang, and Q. V. Le, "Efficientdet: Scalable and efficient object detection," in *Proc. IEEE Conf. Comput. Vis. Pattern Recognit.*, 2020, pp. 10781–10790.
[85] M. Tan and Q. Le, "Efficientnet: Rethinking model scaling for convolutional neural networks," in *Proc. Int. Conf. Mach. Learn.*, 2019, pp. 6105–6114.
[86] K. Kim and H. S. Lee, "Probabilistic anchor assignment with iou prediction for object detection," in *Proc. Eur. Conf. Comput. Vis.*, 2020, pp. 355–371.
[87] H. Zhang, Y. Wang, F. Dayoub, and N. Sunderhauf, "VarifocalNet: An IOU-aware dense object detector," in *Proc. IEEE Conf. Comput. Vis. Pattern Recognit.*, 2021, pp. 8514–8523.
[88] S. J. Pan and Q. Yang, "A survey on transfer learning," *IEEE Trans. Knowl. Data Eng.*, vol. 22, no. 10, pp. 1345–1359, Oct. 2010.
[89] H. Rezatofighi, N. Tsoi, J. Gwak, A. Sadeghian, I. Reid, and S. Savarese, "Generalized intersection over union: A metric and a loss for bounding box regression," in *Proc. IEEE Conf. Comput. Vis. Pattern Recognit.*, 2019, pp. 658–666.

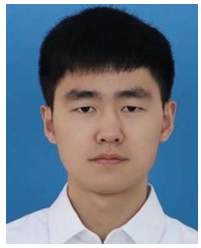

Chi Zhang received the B.S. degree in remote sensing from the Shandong University of Science and Technology, Qingdao, China, in 2018, and the M.S. degree in geomatics engineering from the China University of Petroleum, Qingdao, China, in 2021, where he is currently working toward the Ph.D. degree in geomatics engineering.

His research interests include algorithms for ship detection and classification in SAR remote imagery using deep learning and machine learning.

Xi Zhang received the B.S. degree in information systems from the Qingdao University of Science and Technology, Qingdao, China, in 2005, and the M.S. degree in signal and information processing and the Ph.D. degree in computer science from the Ocean University of China, Qingdao, China, in 2008 and 2011, respectively.

He is currently a Professor with the Laboratory of Marine Physics and Remote Sensing, First Institute of Oceanography, Ministry of Natural Resources, Qingdao, China. He participated in several land-based and airborne geoscientific field studies, among which a number of campaigns were related to sea ice studies in the Bohai Sea. His research interests include microwave remote sensing of sea ice, numerical modeling of sea ice scattering, and synthetic aperture radar data analysis.

Jie Zhang received the B.S. and M.S. degrees in mathematics from Inner Mongolia University, Urumqi, China, in 1984 and 1987, respectively, and the Ph.D. degree in applied mathematics from Tsinghua University, Beijing, China, in 1993.

He is the Director of the Laboratory of Marine Physics and Remote Sensing, the First Institute of Oceanography, Ministry of Natural Resources, Qingdao, China. He has a broad interest in marine physics and remote sensing applications. His research interests include SAR retrieval of ocean dynamics process and SAR detection of marine targets, ocean hyperspectral remote sensing, high-frequency surface-wave radar ocean detection technique, and integration of marine remote sensing application system.

Dr. Zhang has served as a member of multiple domestic/international committees and a Principle Investigator/Coinvestigator of many projects from the National Science Foundation of China, State High-Tech Development Plan (863), and other funding agencies. He has been the Supervisor for nearly 40 Ph.D. students and has published more than 200 papers.

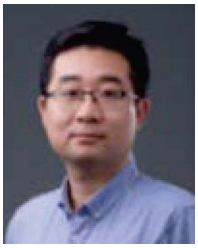

Gui Gao (Member, IEEE) received the B.S. degree in information engineering, the M.S. and Ph.D. degrees in remote sensing information processing from the National University of Defense Technology (NUDT), Changsha, China, in 2002, 2003, and 2007, respectively.

Since 2007, he has been an Associate Professor with the Faculty of Information Engineering, School of Electronic Science and Engineering, NUDT. Since 2017, he has been with the Faculty of Geosciences and Environmental Engineering, Southwest Jiaotong University, Chengdu, China, where he is a Professor. He is also a Guest Professor with the College of Traffic Engineering, Hunan University of Technology, Zhuzhou, China. He has authored over 100 journal and conference articles and has written four books and an English chapter. His research interests include radar signal processing, interferometric synthetic aperture radar, target detection, marine environment, and SAR ground moving target indication.

Yongshou Dai received the B.S. degree in production process automation from the University of Petroleum, Dongying, China, in 1986, the M.Eng. degree in computer application from Northern Jiaotong University, Beijing, China, in 1991, and the Ph.D. degree in control theory and control engineering from the University of Science and Technology Beijing, China, in 2007.

He is currently a Professor with the College of Oceanography and Space Informatics, China University of Petroleum (East China), Qingdao, China. His research interests include seismic signal processing, marine environment monitoring, and information processing.

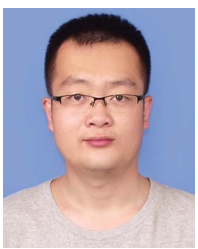

Genwang Liu received the B.S. and M.S. degrees in automation from Inner Mongolia University, Inner Mongolia, China, in 2011 and 2014, respectively, and the Ph.D. degree in computer science from the Ocean University of China, Qingdao, China, in 2017.

He is currently a Research Associate with the Laboratory of Marine Physics and Remote Sensing, the First Institute of Oceanography, Ministry of Natural Resources, Qingdao, China. His research interests include ship SAR Detection and classification, polarimetric SAR and marine applications, SAR simulation and image interpretation.

Yongjun Jia received the B.S. degree in information and computing science from Inner Mongolia University, Inner Mongolia, China, in 2004, the MA.Sc. and Ph.D. degrees in physical oceanography from the Institute of Oceanology, Chinese Academy of Sciences, Beijing, China, in 2007 and 2010, respectively.

He was a Deputy Chief Designer of the ground application system for the HY-2 satellites and new generational ocean dynamic satellites, where he organized the framework and managed the construction of the ground application system for the Chinese ocean dynamic satellites. His research interests include ocean satellite data processing, remote sensing of the ocean, and associated applications.

Xiaochen Wang received the B.S. and M.S. degrees in surveying and mapping sciences from the China University of Petroleum (East China), Qingdao, China, in 2013 and 2016, respectively, and the Ph.D. degree in signal and information processing from the Institute of Remote Sensing and Digital Earth, Chinese Academy of Sciences, Beijing, China, in 2019.

His research interests include SAR imaging mechanism over ocean waves.

Yi Zhang received the Ph.D. degree in signal and information processing from the Chinese Academy of Sciences, Beijing, China, in 2010.

His main study field includes microwave scatterometer ground-based data processing, satellite geolocation, ocean wind retrieval and ocean wind fields applications.

In 2011, he was responsible for the development of geolocation and NRCS data calculation algorithms of the HY-2A Satellite Microwave Scatterometer. He played an important role in developing the entire ground-based data processing system. From 2012 to 2016, he mainly engaged in ground system maintenance, ocean wind fields applications, and so on. He is now the chief designer of the HY-2B/C/D Satellite Microwave Scatterometer ground data processing systems.

Meng Bao received the B.S. and M.S. degrees in geographic information system from Inner Mongolia Normal University, Inner Mongolia, China, in 2011 and 2014, respectively.

She is currently an Engineer with the Laboratory of Marine Physics and Remote Sensing, the First Institute of Oceanography, Ministry of Natural Resources, Qingdao, China. Her research interests include marine microwave remote sensing and polarimetric SAR target detection.